Journal of Biomedical Optics

SPIEDigitalLibrary.org/jbo

Texture analysis of collagen second-harmonic generation images based on local difference local binary pattern and wavelets differentiates human skin abnormal scars from normal scars

Yao Liu
Xiaoqin Zhu
Zufang Huang
Jianyong Cai
Rong Chen
Shuyuan Xiong
Guannan Chen
Haishan Zeng

SPIE

Texture analysis of collagen second-harmonic generation images based on local difference local binary pattern and wavelets differentiates human skin abnormal scars from normal scars

Yao Liu,[a,b] Xiaoqin Zhu,[a,*] Zufang Huang,[a] Jianyong Cai,[a,b] Rong Chen,[a] Shuyuan Xiong,[c] Guannan Chen,[a,b,d,*] and Haishan Zeng[c]

[a]Fujian Normal University, Institute of Laser and Optoelectronics Technology, Fujian Provincial Key Laboratory for Photonics Technology, Key Laboratory of OptoElectronic Science and Technology for Medicine of Ministry of Education, No.32 Shangsan Road, Cangshan District, Fuzhou 350007, China
[b]Fujian Normal University, Department of Network and Communication Engineering, No.32 Shangsan Road, Cangshan District, Fuzhou, 350007, China
[c]Affiliated First Hospital Fujian Medical University, Department of Plastic Surgery, No.20 Chazhong Road, Taijiang District, Fuzhou 350005, China
[d]British Columbia Cancer Agency Research Centre, Imaging Unit–Integrative Oncology Department, 675 West 10th Avenue, Vancouver, British Columbia V5Z 1L3, Canada

Abstract. Quantitative methods for noninvasive diagnosis of scars are a challenging issue in medicine. This work aims to implement a texture analysis method for quantitatively discriminating abnormal scars from normal scars based on second-harmonic generation (SHG) images. A local difference local binary pattern (LD-LBP) operator combined with a wavelet transform was explored to extract diagnosis features from scar SHG images that were related to the alteration in collagen morphology. Based on the quantitative parameters including the homogeneity, directional and coarse features in SHG images, the scar collagen SHG images were classified into normal or abnormal scars by a support vector machine classifier in a leave-one-out cross-validation procedure. Our experiments and data analyses demonstrated apparent differences between normal and abnormal scars in terms of their morphological structure of collagen. By comparing with gray level co-occurrence matrix, wavelet transform, and combined basic local binary pattern and wavelet transform with respect to the accuracy and receiver operating characteristic analysis, the method proposed herein was demonstrated to achieve higher accuracy and more reliable classification of SHG images. This result indicated that the extracted texture features with the proposed method were effective in the classification of scars. It could provide assistance for physicians in the diagnostic process. [DOI: 10.1117/1.JBO.20.1.016021]

Key words: normal scar; abnormal scar; second-harmonic generation; texture features; local difference local binary pattern; wavelet transform.

Paper 140590RR received Sep. 14, 2014; accepted for publication Dec. 30, 2014; published online Jan. 22, 2015.

1 Introduction

Scars are areas of fibrosis that replace normal skin secondary to traumatic or surgical injuries.[1] Broadly, scars are divided into two types: physiologic (normal) and pathologic (abnormal) scars. Normal scars resulting from a balanced production and degradation of collagen show no painful symptoms and no dysfunction.[2] Abnormal scars, typically including hypertrophic scars and keloids, are histopathologically characterized by excessive deposition and the disordered arrangement of collagen fibers,[3] causing esthetical dissatisfaction and even turning cancerous.[4] For the variety of collagenous frameworks in scar tissues, the morphological distinctions of collagen in normal scars compared to abnormal scars can help to differentiate types of scars.

Recently, due to many unique advantages such as reduced photobleaching and photodamage as well as high resolution imaging deep into several hundred microns,[5,6] second-harmonic generation (SHG) microscopy has emerged as a potential noninvasive tool for imaging collagen in scar tissues.[7,8] Many researches relied on SHG microscopy to describe collagen organization using empirical observations that were linked to a pathological condition.[9,10] And also, several SHG studies have proposed methodologies for quantifying characteristics of collagen.[11–13] Texture analysis can provide a novel way of achieving these ends. A gray level co-occurrence matrix (GLCM) has been already used in the texture analysis of SHG images,[14,15] but with the limitation of heavy computation.

The local binary pattern (LBP) introduced by Ojala et al.[16] is a widely used texture descriptor because of its low computational burden and rotation invariance.[17] To overcome the drawbacks of analyzing the local grayscale difference, an improved approach referred to as local difference local binary pattern (LD-LBP), was proposed herein for evaluating the homogeneity feature in SHG images to distinguish collagen distribution in scars. Meanwhile, wavelet transform can capture the directional and coarse features in scar SHG images that quantitatively determine the collagen orientation and coarseness. In this study, we

*Address all correspondence to: Guannan Chen, E-mail: edado@fjnu.edu.cn; Xiaoqin Zhu, E-mail: zhuxq@fjnu.edu.cn

0091-3286/2015/$25.00 © 2015 SPIE

combined an LD-LBP operator with a wavelet transform for the texture analysis of scar collagen SHG images. The homogeneity, directional and coarse features of SHG images that are associated with the collagen morphology in scar tissues were simultaneously extracted to differentiate abnormal scars from normal scars. To deal with the classification in the situation of a small example scale, a support vector machine (SVM) classifier was applied using a leave-one-out cross-validation (LOOCV) procedure. In addition, comparisons with other texture analysis methods such as GLCM, wavelet transform, and basic LBP combined with wavelet transform were performed to verify the proposed method.

2 Materials and Methods

2.1 *Tissue Samples*

The *ex vivo* matured human skin scar specimens (30 normal and 30 abnormal scars) were collected during plastic surgery performed on 60 Chinese female patients. The scars were diagnosed based on histological examination by certified pathologists and classified according to the traditional histopathological criteria.[4,18] Prior to study participation, all patients signed an informed consent, and this study was approved by the Institutional Review Board of Fujian Medical University. To protect the tissue samples from metamorphism, we stored them in liquid nitrogen (−196°C) immediately after they were excised from patients. Prior to SHG imaging, the tissues were sectioned in 140-μm thicknesses and sandwiched between a microscope slide and cover glass. To avoid dehydration or shrinkage during the imaging acquisition, a little phosphate-buffered saline (PBS) solution was dripped into the tissue specimen.

2.2 *Second-Harmonic Generation Microscopy*

The SHG imaging was performed on a Zeiss LSM 510 META laser scanning microscope coupled to a mode-locked femtosecond Ti: sapphire laser (Coherent Mira 900-F) operating at 810 nm. The sapphire laser (110 fs, 76 MHz) was used as the excitation light source. An oil immersion objective (×63 and NA = 1.4) was employed for focusing the excitation beam into tissue samples (average power less than 5 mW) and for collecting the backscattered intrinsic SHG signals. The high-resolution (512 × 512 pixels) image was obtained at 2.56 μs per pixel (total: 1.57 s) with a view field of 230.8 μm × 230.8 μm. In this study, one SHG image was collected from each patient, resulting in a total of 60 scar collagen SHG images (30 normal and 30 abnormal) for analysis.

2.3 *Texture Analysis*

2.3.1 *Homogeneity features extracted by local difference local binary pattern*

To characterize the homogeneity features in an image, the local contrast information derived from LD-LBP was used. Given a gray value of central pixel g_c and its neighbors g_p ($p = 0,1,\ldots,P$–1, P is the number of sampling points in a neighborhood), the difference between g_c and g_p can be calculated by $C_p = g_p - g_c$, and the amplitude of C_p is expressed as $S_p = |C_p|$. As an example, Fig. 1(a) shows the 3 × 3 neighborhood with central pixel g_c being 20 and the neighboring pixels g_p are [12, 71, 43, 39, 27, 31, 14, and 6]. The differences in C_p [Fig. 1(b)] are [-8, 51, 23, 19, 7, 11, −6, −14], and the amplitudes S_p are [8, 51, 23, 19, 7, 11, 6, 14], as shown in Fig. 1(c). Then LD-LBP is defined as

(a)

6	14	31
12	20	27
71	43	39

(b)

-14	-6	11
-8		7
51	23	19

(c)

14	6	11
8		7
51	23	19

Fig. 1 (a) 3 × 3 neighborhood with central pixel being 20; (b) the local differences; and (c) the amplitudes of local differences.

$$\text{LD-LBP} = \sum_{p=0}^{P-1} H(S_p - t)2^p, \tag{1}$$

where $H(x) = \begin{cases} 1, x \geq 0 \\ 0, x < 0 \end{cases}$ and t is a threshold to be adaptively determined. Here, we set t as the mean value of S_p from the whole image. The LD-LBP operator is defined in a consistent format with that of the basic LBP operator. Similar to the basic LBP, the rotation invariant version of LD-LBP is also defined to achieve rotation invariant classification. Additionally, the LD-LBP uses a rotation invariant variance measure VAR that characterizes the contrast of local image texture as the representation of homogeneity features

$$\text{VAR} = \sum_{p=0}^{P-1} (g_p - w)^2 / P, \tag{2}$$

where

$$w = \left(\sum_{p=0}^{P-1} g_p \right) / P. \tag{3}$$

Low variance (VAR) occurs in images with homogeneous features, otherwise the *VAR* is higher.

2.3.2 *Directional and coarse features extracted by wavelet transform*

Wavelet transform[19,20] was utilized to evaluate the directional and coarse features in an image. The wavelet transform decomposes an image into four subimages: low–low (LL), low–high (LH), high–low (HL), and high–high (HH). LL is the low-frequency subimage that contains the main information of the decomposed image. LH, HL, and HH are three high-frequency subimages which are horizontal, vertical, and oblique subimages, respectively. The wavelet energy (E) was estimated by summing the squares of all coefficients $p(i,j)$ from each subimage with dimensions $M \times N$

$$E = \sum_{i=1}^{M} \sum_{j=1}^{N} [p(i,j)]^2. \tag{4}$$

The distribution of energy (E) in each subimage can determine the image directionality. The large energy value represents the main direction of the texture.

For an image with a coarse texture, the energy is mainly concentrated in the low-frequency subimage, while for an image with a thin or complex texture, the energy is mainly

concentrated in the high-frequency subimage.[21] Thus, the energy ratio (E_r) in the low-frequency subimage was calculated to investigate the coarse features of an image, given by

$$E_r = \frac{E_{\mathrm{LL}}}{E_{\mathrm{LL}} + E_{\mathrm{LH}} + E_{\mathrm{HL}} + E_{\mathrm{HH}}} \times 100\%, \tag{5}$$

where E_{LL}, E_{LH}, E_{HL}, and E_{HH} represent the energy (E) in LL, LH, HL, and HH subimages, respectively. The energy ratio (E_r) is higher in images with coarse features and lower for those with thin or complex features.

2.3.3 *Combination of local difference local binary pattern and wavelet transform*

To simultaneously obtain the homogeneity, directional and coarse features, LD-LBP and wavelet transform were combined for analysis. The steps of the algorithm are given as follows:

Step 1: Transform the original SHG image (512×512 pixels) into a grayscale image.
Step 2: Encode the grayscale image by LD-LBP, and calculate LD-LBP variance (VAR) according to Eq. (2).
Step 3: Encode the LD-LBP image by wavelet transform, and calculate the energy (E_{LL}, E_{LH}, E_{HL} and E_{HH}) in each subimage and energy ratio (E_r) in the low-frequency subimage according to Eqs. (4) and (5).
Step 4: Combine the above texture parameters to compose the characteristic vector of each image: [VAR, E_{LL}, E_{LH}, E_{HL}, E_{HH}, and E_r].
Step 5: Employ Gaussian normalization[22] to avoid deviation caused by the different physical meaning and the range of each texture parameter. Supposing that the initial characteristic vector is $[f_1, f_2, \ldots, f_n]$, the normalized characteristic vector $[F_1, F_2, \ldots, F_n]$ is calculated by $F_i = (F_i' + 1)/2$, where $F_i' = (f_i - e)/3\sigma$ (e is the mean, and σ is the standard deviation of the initial characteristic vector).

2.4 *Classification*

An SVM classifier was used to test the ability of the texture parameters to classify the SHG images into normal or abnormal.[23–25] Given a training sample set $[(x_i, y_i)]_{i=1}^n$, where x_i denotes the training vector, $x_i \in R^n$ and y_i denote the corresponding class label, $y_i \in \{1, -1\}$, and n denotes the total number of the training sample. SVM finds the solution of the following optimization problem

$$\begin{aligned} &\underset{w,b,\xi}{\mathrm{Minimize}} \frac{1}{2}\langle w \cdot w\rangle + C\sum_{i=1}^{n}\xi_i, \\ &\text{Subject to: } y_i(\langle w \cdot x_i\rangle + b) + \xi_i - 1 \geq 0, \end{aligned} \tag{6}$$

where C is a penalty parameter of the error term, ξ_i is the nonnegative slack variable, w is the normal vector of the hyperplane, and b is the offset of the hyperplane. Then, SVM finds the linearly separating hyperplane with the maximal marginal in a higher dimensional space. A kernel function $K(x_i, x_j) = \varphi(x_i)^T\varphi(x_j)$ is used to map the training sample into a higher dimensional feature space. In our study, the radial basis function was chosen as the kernel of the SVM.

Moreover, the LOOCV procedure was used to address the drawback of the small-sized sample.[26,27] Each time one single sample was considered as the validation data and the other samples were considered as the training data. In this work, we have a total of 60 scar collagen SHG images (30 normal and 30 abnormal). The procedure was repeated 60 times until every sample was used as the validation data.

2.5 *Statistical Analysis*

For statistical analysis, a total of 30 normal and 30 abnormal scar collagen SHG images were measured for texture analysis. Statistical analyses were performed by using the MATLAB® (version 2010b) software. Quantitative data were presented as a mean value with its standard deviation indicated (mean ± SD) and compared using the Student's t-test analysis. Differences were considered to be statistically significant when the p-values were less than 0.05.

3 Results

3.1 *Collagen Second-Harmonic Generation Images of Human Skin Scars*

Representative high-resolution collagen SHG images from human normal and abnormal scars are shown in Figs. 2(a) and 2(b), respectively. This presents a great difference in the morphological structure of the collagen between the normal and abnormal scars. As we can see from Fig. 2(a), large and

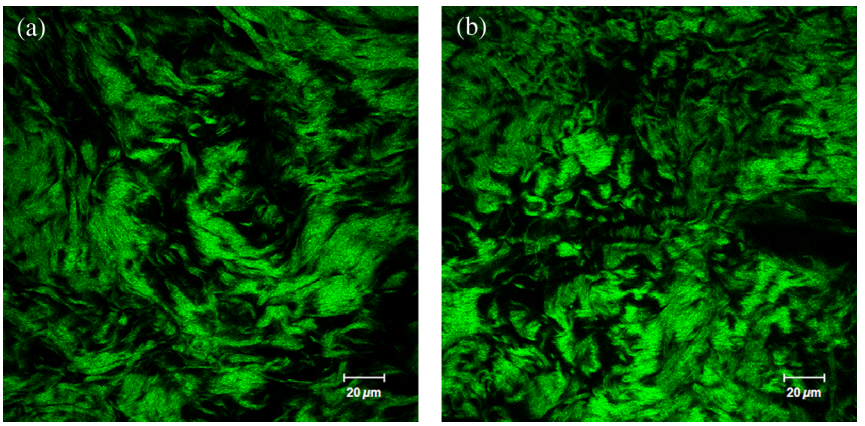

Fig. 2 Collagen second-harmonic generation (SHG) images in human (a) normal and (b) abnormal scars. Images are 512×512 pixels.

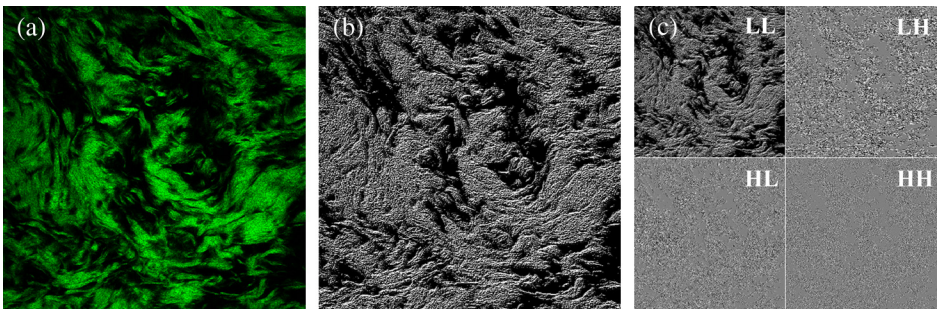

Fig. 3 The decomposition process of collagen in an SHG image. (a) Original collagen SHG image of normal scar. (b) The local difference local binary pattern (LD-LBP) transformed image in gray scale from (a). (c) The four subimages by one-level wavelet transform decomposed from (b).

coarse collagen bundles with a well-regulated distribution and well-defined orientation in the normal scar are well identified. In contrast, a less organized and disordered collagen structure characterized by thinner but more complex fibril bundles are clearly seen in the abnormal scar [Fig. 2(b)]. All these observations are well consistent with the previous description of normal or abnormal scars.[28,29]

3.2 *Quantification of Collagen in Human Skin Scars*

In order to quantitatively characterize the collagen morphology in normal and abnormal scars such as collagen distribution, collagen orientation, and collagen coarseness, we applied detailed texture analysis based on LD-LBP and wavelet transform to collagen SHG images. Texture parameters including homogeneity, directional and coarse features of SHG images were extracted. Demonstrated in Fig. 3 is the decomposition process of the collagen SHG images, including an original collagen SHG image of normal scar [Fig. 3(a)], the corresponding LD-LBP transformed image in gray scale [Fig. 3(b)], and the four subimages by one-level wavelet transform decomposed from the LD-LBP image [Fig. 3(c)].

3.2.1 *Homogeneity feature*

Figure 4 presents the LD-LBP variances of collagen SHG images from normal and abnormal scars, showing a much smaller value of normal scar SHG images compared to abnormal scar SHG images (0.04 ± 0.01 versus 0.55 ± 0.35; $p < 0.05$). Quantitatively analyzed result indicates that the normal scars have a more homogeneous collagen morphology than the abnormal scars.

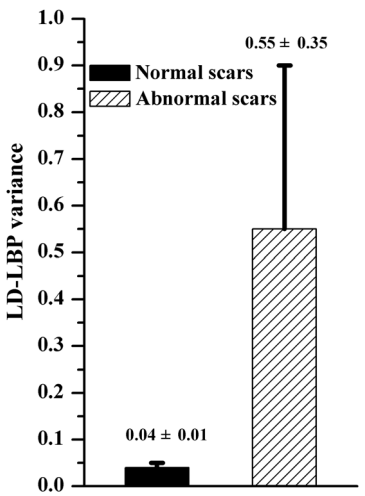

Fig. 4 LD-LBP variances of collagen SHG images from normal and abnormal scars. Error bars indicate calculated standard deviations.

3.2.2 *Directional and coarse features*

Figure 5 gives the energy values in each subimage on both normal and abnormal scar SHG images. By comparing energy values in each subimage, it can be seen that the energy is mainly concentrated in the LL subimage compared to LH, HL, or HH subimage, for both normal (2.16 ± 0.09 versus 0.44 ± 0.03, 0.26 ± 0.04, or 0.20 ± 0.03; $p < 0.05$) and abnormal scar collagen SHG images (1.72 ± 0.11 versus 0.69 ± 0.09, 0.32 ± 0.02, or 0.18 ± 0.02; $p < 0.05$). Moreover, texture details are mainly distributed in the LH subimage and less distributed in HL or HH subimages for both normal (0.44 ± 0.03 versus 0.26 ± 0.04, or 0.20 ± 0.03; $p < 0.05$) and abnormal scar collagen SHG images (0.69 ± 0.09 versus 0.32 ± 0.02, or 0.18 ± 0.02; $p < 0.05$).

Energy ratios in the low-frequency subimage are depicted in Fig. 6. This clearly shows that energy ratios in the low-frequency subimage of normal scar SHG images are higher than those of abnormal scar SHG images ($70.55 \pm 1.93\%$ versus $59.27 \pm 0.46\%$; $p < 0.05$). These statistical results are consistent with the observation that the collagen arrangement within normal scars is ordered and coarser compared to abnormal scars.

3.3 *Optimal Wavelet and Decomposition Level*

Table 1 describes the accuracy of the SVM classifier in the LOOCV procedure based on texture parameters of LD-LBP

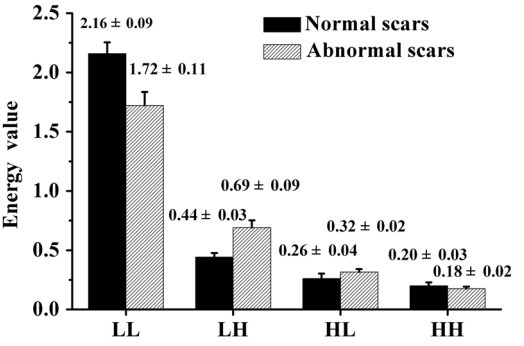

Fig. 5 Energy values in each subimage of collagen SHG images from normal and abnormal scars. Error bars indicate calculated standard deviations.

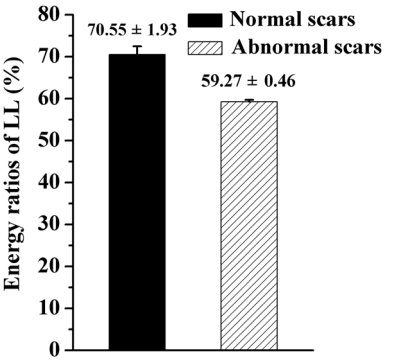

Fig. 6 Energy ratios in low-frequency subimage of collagen SHG images from normal and abnormal scars. Error bars indicate calculated standard deviations.

Table 1 Accuracy of support vector machine (SVM) classifier in the leave-one-out cross-validation (LOOCV) procedure based on texture parameters of local difference local binary pattern (LD-LBP) combined with Haar, Daubechies, Symlets, and Morlet wavelet transform.

Group	LD-LBP + Haar (%)	LD-LBP + Daubechies (%)	LD-LBP + Symlets (%)	LD-LBP + Morlet (%)
Normal	90.0	90.0	83.3	86.7
Abnormal	90.0	86.7	86.7	90.0
Overall	90.0	88.3	85.0	88.3

combined with Haar, Daubechies, Symlets, and Morlet wavelet transform. As can be seen from the table, the overall accuracy of the SVM classifier is relatively higher when LD-LBP is combined with the Haar wavelet. Moreover, Haar wavelet is fast in speed and describes detailed features,[30] which were adopted in this study.

Listed in Table 2 is the accuracy of the SVM classifier in the LOOCV procedure based on the texture parameters of LD-LBP combined with an n-level Haar wavelet transform ($n = 1, 2, 3$). It can be observed that the SVM classifier has an overall accuracy of 90.0% when LD-LBP is combined with one-level Haar wavelet. The accuracy drops to 73.3% and 71.7% when a two-level or three-level Haar wavelet was used. Therefore, a one-level Haar wavelet transform was selected in this analysis.

3.4 *Comparison with Other Methods*

To evaluate the effectiveness of the proposed method for scar discrimination, the SVM classifier in the LOOCV procedure

Table 2 Accuracy of SVM classifier in the LOOCV procedure based on texture parameters of LD-LBP combined with one-level, two-level, and three-level Haar wavelet transform.

Group	LD-LBP + one-level Haar (%)	LD-LBP + two-level Haar (%)	LD-LBP + three-level Haar (%)
Normal	90.0	86.7	83.3
Abnormal	90.0	60.0	60.0
Overall	90.0	73.3	71.7

Table 3 Comparison of the accuracy of LD-LBP + Haar wavelet transform to other methods.

Group	WND-CHARM (%)	GLCM (%)	Haar (%)	Basic LBP + Haar (%)	LD-LBP + Haar (%)
Normal	83.3	80.0	83.3	86.7	90.0
Abnormal	66.7	30.0	23.3	50.0	90.0
Overall	75.0	55.0	53.3	68.3	90.0

was trained and applied to classify collagen SHG images of normal and abnormal scar tissues using GLCM, Haar wavelet transform, basic LBP combined with Haar wavelet transform, and the proposed method combining LD-LBP and Haar wavelet transform texture parameters, respectively. Additionally, a multipurpose image classifier called WND-CHARM was also used for comparison.[31] Results are shown in Table 3. Using the GLCM,[32,33] four texture features including contrast, correlation, energy, and homogeneity were extracted from the scar collagen SHG images and analyzed using the texture average of four directions (0 deg, 45 deg, 90 deg, 135 deg) with distance, $d = 10$. It can be seen from Table 3 that the SVM classifier has a higher accuracy when combined LD-LBP and Haar wavelet transform parameters were included in the classification model, while a lower accuracy is obtained when GLCM or Haar wavelet transform was independently used, respectively. The basic LBP combined with a Haar wavelet transform does not give a satisfactory performance for distinguishing abnormal scars from normal scars. In addition, WND-CHARM was less effective than the proposed method specifically designed for texture classification of scar SHG images.

Figure 7 compares the receiver operating characteristic (ROC) curves[34] with the LOOCV procedure generated by texture parameters from the GLCM, Haar wavelet transform, basic LBP combined with Haar wavelet transform, and the proposed

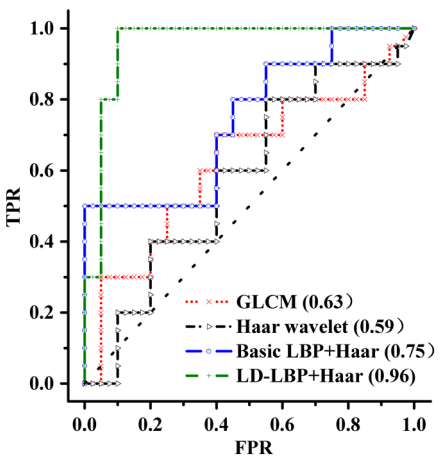

Fig. 7 Receiver operating characteristic (ROC) curves for texture parameters from the four texture analysis methods including gray level co-occurrence matrix (GLCM), Haar wavelet transform, basic LBP + Haar wavelet transform, and LD-LBP + Haar wavelet transform. The area under the ROC curve is 0.96 for texture parameters (LD-LBP + Haar), 0.75 for texture parameters (basic LBP + Haar), 0.59 for Haar wavelet parameters and 0.63 for GLCM parameters.

method. The area under the ROC curve (AUC) is a measure of the overall diagnostic performance.[35] It is seen from Fig. 7 that the accuracy of the SVM classifier, as represented by the AUC, is determined to be 0.96 when LD-LBP was combined with Haar wavelet transform parameters for classification. These values drop to 0.75, 0.63, and 0.59 when the combined basic LBP and Haar wavelet transform parameters, the GLCM parameters or the Haar wavelet transform parameters were independently used, respectively. The diagonal line $y = x$ is the expected ROC curve of a random guesser (with AUC = 0.5).

4 Discussion

In this paper, the combination of LD-LBP and wavelet transform was proposed to characterize the homogeneity, directional and coarse features in SHG images of human skin abnormal scars distinguished from normal scars. First, using the LD-LBP variance, we quantitatively evaluated the collagen distribution within normal and abnormal scar tissues. The comparison of the LD-LBP variances of normal and abnormal scar collagen SHG images (Fig. 4) demonstrated that the texture distribution in the normal scar SHG images was more homogeneous compared to abnormal scar SHG images. This verified the point that the distribution of the collagen in normal scars is better-regulated than that of abnormal scars, supported by the observations in collagen SHG images from normal and abnormal scars (Fig. 2). Second, to investigate the differences in the collagen orientation or coarseness between normal and abnormal scars, we calculated energy values of each subimage (Fig. 5) and energy ratios in the low-frequency subimages of SHG images (Fig. 6). The results indicated that normal scar SHG images had more ordered and coarser textures compared to the abnormal scar SHG images. The provided interpretation supported the previous reports that the collagen fibers in normal scars are better oriented and coarser than those of abnormal scars.[12,28,36] In addition, to determine the optimal wavelet and decomposition level, we evaluated the texture parameters of LD-LBP combined with Haar, Daubechies, Symlets, and Morlet wavelet (Table 1), and one-level, two-level, and three-level Haar wavelet transform via the SVM classifier with the LOOCV procedure (Table 2). Based on the data presented in Tables 1 and 2, it was quite evident that the one-level Haar wavelet achieved the highest accuracy.

On the other hand, the accuracy of the SVM classifier based on texture parameters extracted from the proposed method that combined LD-LBP and Haar wavelet transform was compared to other methods including GLCM, Haar wavelet transform, the basic LBP combined with Haar wavelet transform, and WND-CHARM (Table 3). Overall, the SVM classifier using the texture parameters from the proposed method gave better accuracy than WND-CHARM, GLCM, Haar wavelet transform, or the basic LBP combined with Haar wavelet. Finally, the ROC analysis further evaluated the performance of the proposed method (Fig. 7). The ROC curve based on LD-LBP combined with Haar wavelet transform parameters achieved the highest AUC values (AUC = 0.96). This indicates that our methodology is effective in differentiating abnormal scars from normal scars. It may enable a better understanding of the pathophysiology of scars. Texture analysis for quantifying scar collagen morphology is a work in progress and shows feasibility in scar diagnosis. We have reason to believe that it may provide a valuable tool for studying scars.

5 Conclusion

In conclusion, we have demonstrated the feasibility of quantitative discrimination between human normal and abnormal scars based on texture analysis combining LD-LBP and Haar wavelet transform derived from SHG images. The homogeneity, directional and coarse features that are associated with the collagen morphology in scars demonstrated the differences between normal and abnormal scar SHG images. Using the SVM classifier with the LOOCV procedure and ROC analysis, the accuracy was demonstrated to be improved with combined LD-LBP and Haar wavelet transform parameters compared to the case when the GLCM, the Haar wavelet transform or the basic LBP combined with Haar wavelet parameters were independently used. Although our study is only a proof of concept with a limited sample size, its implication is that the texture analysis of SHG images could have clinical potential in differentiating abnormal scars from normal scars, and can also help plastic surgeons and dermatologists to identify optimal therapeutic options to cure scars.

Acknowledgments

This work was supported by the Program for Changjiang Scholars and Innovative Research Team in University (IRT1115), and the National Natural Science Foundation of China (Grant Nos. 81101110, 81101209, and 61308113).

References

1. A. Bayat, D. A. McGrouther, and M. W. J. Ferguson, "Skin scarring," *Brit. Med. J.* **326**, 88–92 (2003).
2. R. L. Bang et al., "Trace elements content in serum, normal skin, and scar tissues of keloid and normal scar patients," *J. Trace. Elem. Exp. Med.* **15**, 57–66 (2002).
3. S. S. Tsao et al., "Scar management: keloid, hypertrophic, atrophic and acne scars," *Semin. Cutan. Med. Surg.* **21**, 46–75 (2002).
4. D. Wolfram et al., "Hypertrophic scars and keloids—a review of their pathophysiology, risk factors, and therapeutic management," *Dermatol. Surg.* **35**, 171–181 (2009).
5. X. Han et al., "Second harmonic properties of tumor collagen: determining the structural relationship between reactive stroma and healthy stroma," *Opt. Express* **16**, 1846–1859 (2008).
6. O. Nadiarnykh et al., "Alterations of the extracellular matrix in ovarian-cancer studied by second harmonic generation imaging microscopy," *BMC Cancer* **10**, 1–14 (2010).
7. J. Chen et al., "Multiphoton microscopy study of the morphological and quantity changes of collagen and elastic fiber components in keloid disease," *J. Biomed. Opt.* **16**, 051305 (2011).
8. X. Zhu et al., "Quantified characterization of human cutaneous normal scar using multiphoton microscopy," *J. Biophotonics* **3**, 108–116 (2010).
9. P. J. Campagnola and L. M. Loew "Second-harmonic imaging microscopy for visualizing biomolecular arrays in cells, tissues and organisms," *Nat. Biotechnol.* **21**, 1356–1360 (2003).
10. A. M. Pen et al., "Three-dimensional investigation and scoring of extracellular matrix remodeling during lung fibrosis using multiphoton microscopy," *Microsc. Res. Tech.* **70**, 162–170 (2007).
11. P. F. Lee, A. T. Yeh, and K. J. Bayless, "Nonlinear optical microscopy reveals invading endothelial cells anisotropically alter three-dimensional collagen matrices," *Exp. Cell Res.* **315**, 396–410 (2009).
12. G. Chen et al., "Nonlinear spectral imaging of human hypertrophic scar based on two-photon excited fluorescence and second-harmonic generation," *Brit. J. Dermatol.* **161**, 48–55 (2009).
13. P. J. Su et al., "The discrimination of type I and type II collagen and the label-free imaging of engineered cartilage tissue," *Biomaterials* **31**, 9415–9421 (2010).
14. L. B. Mostaço-Guidolin et al., "Evaluation of texture parameters for the quantitative description of multimodal nonlinear optical images from atherosclerotic rabbit arteries," *Phys. Med. Biol.* **56**, 5319–5334 (2011).

15. W. Zheng et al., "Diagnostic value of nonlinear optical signals from collagen matrix in the detection of epithelial precancer," *Opt. Lett.* **36**, 3620–3622 (2011).
16. T. Ojala, M. Pietikainen, and T. Maenpaa, "Multiresolution gray-scale and rotation invariant texture classification with local binary patterns," *IEEE Trans. Pattern Anal. Mach. Intell.* **24**, 971–987 (2002).
17. L. Srensen, S. B. Shaker, and M. De Bruijne, "Quantitative analysis of pulmonary emphysema using local binary patterns," *IEEE Trans. Med. Imaging* **29**, 559–569 (2010).
18. F. B. Niessen et al., "On the nature of hypertrophic scars and keloids: a review," *Plast. Reconstr. Surg.* **104**, 1435–1458 (1999).
19. S. Arivazhagan and L. Ganesan, "Texture classification using wavelet transform," *Pattern Recognit. Lett.* **24**, 1513–1521 (2003).
20. M. Alvarez et al., "Application of wavelets to the evaluation of phantom images for mammography quality control," *Phys. Med. Biol.* **57**, 7177–7190 (2012).
21. J. Zhang, X. Wang, and S. Palmer, "Objective grading of fabric pilling with wavelet texture analysis," *Textile Res. J.* **77**, 871–879 (2007).
22. Y. Rui et al., "Relevance feedback: a power tool for interactive content-based image retrieval," *IEEE Trans. Circ. Syst. Video Technol.* **8**, 644–655 (1998).
23. M. Pal and G. M. Foody, "Feature selection for classification of hyperspectral data by SVM," *IEEE Trans. Geosci. Remote* **48**, 2297–2307 (2010).
24. C. Feng and L. P. Wang, "Applications of support vector machines to cancer classification with microarray data," *Int. J. Neural. Syst.* **15**, 475–484 (2005).
25. A. H. Khandoker, M. Palaniswami, and C. K. Karmakar, "Support vector machines for automated recognition of obstructive sleep apnea syndrome from ECG recordings," *IEEE Trans. Inf. Technol. Biomed.* **13**, 37–48 (2009).
26. A. Johansson, M. Karlsson, and T. Nyholm, "CT substitute derived from MRI sequences with ultrashort echo time," *Med. Phys.* **38**, 2708–2714 (2011).
27. J. Wang et al., "MicroRNAs in plasma of pancreatic ductal adenocarcinoma patients as novel blood-based biomarkers of disease," *Cancer Prev. Res.* **2**, 807–813 (2009).
28. N. V. Kamath et al., "A light microscopic and immunohistochemical evaluation of scars," *J. Cutaneous. Pathol.* **29**, 27–32 (2002).
29. V. Da Costa et al., "Nondestructive imaging of live human keloid and facial tissue using multiphoton microscopy," *Arch. Facial Plast. Surg.* **10**, 38–43 (2008).
30. I. A. Eckley, G. P. Nason, and R. L. Treloar, "Locally stationary wavelet fields with application to the modelling and analysis of image texture," *J. Roy. Stat. Soc. C-App.* **59**, 595–616 (2010).
31. N. Orlov et al., "WND-CHARM: Multi-purpose image classification using compound image transforms," *Pattern. Recognition. Lett.* **29**, 1684–1693 (2008).
32. R. M. Haralick, K. Shanmugam, and I. Dinstein, "Textural features for image classification," *IEEE Trans. Syst. Man. Cybern.* **3**, 610–621 (1973).
33. J. M. Y. Willaime et al., "Quantification of intra-tumour cell proliferation heterogeneity using imaging descriptors of 18F fluorothymidine-positron emission tomography," *Phys. Med. Biol.* **58**, 187–203 (2013).
34. T. Fawcett, "An introduction to ROC analysis," *Pattern Recognit. Lett.* **27**, 861–874 (2006).
35. A. Jiménez-Valverde, "Insights into the area under the receiver operating characteristic curve (AUC) as a discrimination measure in species distribution modeling," *Global Ecol. Biogeogr.* **21**, 498–507 (2012).
36. R. P. Abergel et al., "Biochemical composition of the connective tissue in keloids and analysis of collagen metabolism in keloid fibroblast cultures," *J. Invest. Dermatol.* **84**, 384–390 (1985).

Yao Liu is a postgraduate student at the Institute of Laser and Optoelectronics Technology, Key Laboratory of OptoElectronic Science and Technology for Medicine of Ministry of Education at Fujian Normal University. Her major research is image processing.

Xiaoqin Zhu is an associate professor working at Key Laboratory of OptoElectronic Science and Technology for Medicine of Ministry of Education at Fujian Normal University. Her main research interests include nonlinear spectroscopy and biomedical imaging.

Zufang Huang is an assistant research fellow at the Key Laboratory of OptoElectronic Science and Technology for Medicine of the Ministry of Education at Fujian Normal University. His research experiences include microscopic imaging and Raman spectroscopy in biomedical research.

Jianyong Cai is an associate professor working at the Key Laboratory of OptoElectronic Science and Technology for Medicine of Ministry of Education at Fujian Normal University. His research experiences include color image processing and moving target recognition.

Rong Chen is a professor and director of the Key Laboratory of OptoElectronic Science and Technology for Medicine of Ministry of Education at Fujian Normal University. He has engaged in research about laser medical instrument, optical fiber technology, and laser application technology for 30 years. His current research interests include biomedical optics.

Shuyuan Xiong is a chief physician working at the Department of Plastic Surgery, the First Affiliated Hospital of Fujian Medical University, China. His major research field is the treatment of wound healing at plastic surgery.

Guannan Chen is an associate professor working at the Key Laboratory of OptoElectronic Science and Technology for Medicine of Ministry of Education at Fujian Normal University. His main research interests include image processing and spectrum signal processing in biomedical research.

Haishan Zeng is a distinguished scientist working with the Imaging Unit-Integrative Oncology Department of the British Columbia Cancer Agency Research Centre and a professor of dermatology, pathology, and physics of the University of British Columbia. His research has been focused on developing optical imaging and spectroscopy techniques for improving early cancer detection. He has published over 111 referred journal papers, 8 book chapters, and has 21 granted patents.